



HAL
open science

Pd Supported on Pr-Rich Cerium-Zirconium-Praseodymium Mixed Oxides for Propane and CO Oxidation

Simon Fahed, Rémy Pointecouteau, M. Aouine, A. Boreave, S. Gil, Philippe Bazin, Alain Demourgues, Marco Daturi, P. Vernoux

► **To cite this version:**

Simon Fahed, Rémy Pointecouteau, M. Aouine, A. Boreave, S. Gil, et al.. Pd Supported on Pr-Rich Cerium-Zirconium-Praseodymium Mixed Oxides for Propane and CO Oxidation. *Catalysts*, 2022, 12 (8), 827 (19 p.). 10.3390/catal12080827 . hal-03778685

HAL Id: hal-03778685

<https://hal.science/hal-03778685>

Submitted on 19 Oct 2022

HAL is a multi-disciplinary open access archive for the deposit and dissemination of scientific research documents, whether they are published or not. The documents may come from teaching and research institutions in France or abroad, or from public or private research centers.

L'archive ouverte pluridisciplinaire **HAL**, est destinée au dépôt et à la diffusion de documents scientifiques de niveau recherche, publiés ou non, émanant des établissements d'enseignement et de recherche français ou étrangers, des laboratoires publics ou privés.

Article

Pd Supported on Pr-Rich Cerium–Zirconium–Praseodymium Mixed Oxides for Propane and CO Oxidation

Simon Fahed^{1,2}, Rémy Pointecouteau^{3,4}, Mimoun Aouine¹, Antoinette Boreave¹, Sonia Gil¹ , Philippe Bazin², Alain Demourgues³, Marco Daturi² and Philippe Vernoux^{1,*}

¹ Univ Lyon, Université Claude Bernard Lyon 1, CNRS, IRCELYON, 69626 Villeurbanne, France; simon.fahed@ircelyon.univ-lyon1.fr (S.F.); mimoun.aouine@ircelyon.univ-lyon1.fr (M.A.); antoinette.boreave@ircelyon.univ-lyon1.fr (A.B.); sonia.gil@ircelyon.univ-lyon1.fr (S.G.)

² ENSICAEN, UNICAEN, CNRS, Laboratoire Catalyse et Spectrochimie, Normandie Université, 14050 Caen, France; philippe.bazin@ensicaen.fr (P.B.); marco.daturi@ensicaen.fr (M.D.)

³ CNRS, Université de Bordeaux, ICMCB, 87 Avenue du Dr. Albert Schweitzer, 33608 Pessac, France; remy.pointecouteau@univ-poitiers.fr (R.P.); alain.demourgues@icmcb.cnrs.fr (A.D.)

⁴ Institut de Chimie des Milieux et Matériaux de Poitiers (IC2MP), Université de Poitiers, CNRS UMR 7285, TSA51106, CEDEX 9, 86073 Poitiers, France

* Correspondence: philippe.vernoux@ircelyon.univ-lyon1.fr; Tel.: +33-472-431-587

Abstract: The activity of emission control catalysts must be improved in urban mode at low temperatures. One possible way is to tailor the metal-support interaction between platinum group metals (PGMs) and ceria to stabilize small clusters or single atoms, optimizing the utilization of costly PGMs. In this study, a small loading of Pd (<0.2 wt.%) was dispersed on Pr-rich cerium–zirconium–praseodymium mixed oxides (CZP45: Ce_{0.45}Zr_{0.10}Pr_{0.45}O_{2-x}). After the initial calcination at 800 °C, Pd was mainly in the form of dispersed isolated cations which were found to be efficient for low-temperature CO oxidation but inactive for propane combustion. Nevertheless, a pre-reduction step can trigger the formation of Pd nanoparticles and promote the propane oxidation. Pd nanoparticles, formed during the reduction step, coupled with the high oxygen mobility of CZP45, lead to outstanding catalytic activity for propane oxidation starting from 250 °C. However, the re-oxidation of Pd nanoparticles and their partial re-dispersion, promoted by the fast oxygen mobility of the mixed oxide, rapidly deactivate the catalysts in lean conditions.

Keywords: mixed cerium oxides; emission control; Pd; single-atom catalysts; bulk oxygen mobility



Citation: Fahed, S.; Pointecouteau, R.; Aouine, M.; Boreave, A.; Gil, S.; Bazin, P.; Demourgues, A.; Daturi, M.; Vernoux, P. Pd Supported on Pr-Rich Cerium–Zirconium–Praseodymium Mixed Oxides for Propane and CO Oxidation. *Catalysts* **2022**, *12*, 827. <https://doi.org/10.3390/catal12080827>

Academic Editors: Pengyi Tang, Ting Zhang, Zhifu Liang and Hong Liu

Received: 8 July 2022

Accepted: 25 July 2022

Published: 27 July 2022

Publisher's Note: MDPI stays neutral with regard to jurisdictional claims in published maps and institutional affiliations.



Copyright: © 2022 by the authors. Licensee MDPI, Basel, Switzerland. This article is an open access article distributed under the terms and conditions of the Creative Commons Attribution (CC BY) license (<https://creativecommons.org/licenses/by/4.0/>).

1. Introduction

Ceria-based oxides are commonly used to support platinum group metal (PGM) nanoparticles in three-way catalytic (TWC) converters and diesel oxidation catalysts (DOCs). These catalytic materials, developed for the aftertreatment of gasoline and diesel engines, are prone to deactivation at high temperatures due to the PGM sintering and collapse of the support [1]. Apart from their thermal stability, TWCs and DOCs need to be active in urban mode at temperatures as low as 150 °C to meet the legislation. Cold start phases are the bottleneck of these technologies, since they account for a significant part of the total emissions. This is particularly an issue for alkanes, which are more difficult to oxidize than CO and alkenes. Both Pd and Pt-based catalysts are similarly attractive and often associated in the composition of TWCs and DOCs, the choice of their respective loading being determined by the price difference. In particular, Pd/CeO₂ catalysts were extensively investigated for CH₄ oxidation and seem to be very promising for low-temperature alkane oxidation. Below 877 °C, the temperature of its decomposition in pure oxygen, PdO is the thermodynamically stable phase. In lean burn conditions, such as encountered in diesel exhausts, PdO is proposed to be the active phase via a Mars–van Krevelen (MVK) mechanism involving oxygen active species on PdO. Their consumption creates vacancies

that are refilled with O atoms from the support [2,3]. Nevertheless, some studies reported that a pre-reduction step can enhance the low temperature activity for methane and propane oxidation of Pd-based catalysts [4–7], indicating that Pd, a combination of Pd/PdO or a new layer of PdO formed at low-temperature on Pd surface (in contrast to bulk PdO) can also play a crucial role. However, this activated state of the catalyst after a reduction step is not stable and it is lost under oxidizing conditions [7]. The dynamic and reversible conversion of Pd into PdO makes the active sites difficult to clearly identify. Oxygen chemisorbed on Pd sites at room temperature can slowly oxidize the surface and sub-surface of Pd clusters to finally form a bulk PdO particle above 350 °C. The kinetic of Pd oxidation at low temperature, typically below 450 °C, depends on many parameters, such as the oxygen partial pressure, the cluster size and nanostructure and the nature of the support. For instance, Pd oxidation into PdO was found to be faster on redox supports such as ceria [3,6]. In addition, the presence of H₂O in the reaction mixture deactivates the Pd-based catalysts for low-temperature CH₄ oxidation. This was explained by strongly adsorbed OH species on PdO, which inhibit the CH₄ adsorption [8]. Pd seems to present more resistance to water inhibition than PdO, due to a different activation mechanism of CH₄. Active pairs of sites are supposed to be a Pd²⁺ cation coupled with a lattice oxygen (Pd²⁺-O²⁻) for PdO or two active oxygen species (O*-O*) chemisorbed on Pd [9]. The alloying of Pd with Pt was found to prevent PdO formation and then to reduce water poisoning [10].

Aside from boosting the oxidation of Pd, ceria is known to maintain a high dispersion of PGMs at high temperature [11–13]. Recent studies [12,14,15], dealing with the control of the metal-support interaction between PGMs and ceria, have demonstrated the possibility to stabilize very small supported Pt and Pd clusters on ceria and even single-atom catalysts (SACs), optimizing the utilization of costly PGMs. Moreover, these SACs exhibit dynamic properties under redox conditions, able to form metal NPs during rich phases that can be re-dispersed in lean atmospheres. For instance, the dynamic response of Pt/CeO₂ SACs can be cycled and exploited to tailor very active Pt clusters, including rafts, for CO oxidation [16,17]. In 2009, the pioneer study of Colussi et al. [18] proved, by using HR-TEM (transmission electron microscopy) and DFT (density functional theory) calculations, the ability of ceria to stabilize Pd atoms after a high-temperature calcination at 900 °C in a square planar [PdO₄] surface superstructure, similar to that reported for Pt/CeO₂ [19]. According to You et al. [20], a high surface concentration of oxygen vacancies promotes the full dispersion of isolated Pd species on ceria. Spezzati et al. [21] have determined the energy barriers of diffusion of Pd and PdO₂ on the CeO₂(111) surface to show that isolated PdO₂ species are stable in oxidizing conditions, while the formation of Pd clusters is favorable in rich atmospheres. They have prepared, by a conventional hydrothermal preparation route, a Pd/CeO₂(111) SAC in which the presence of single atoms was confirmed by aberration-corrected TEM and EXAFS. Interestingly, this Pd/CeO₂ SAC was found to be very active for CO oxidation, reaching a full conversion from 170 °C. In situ CO-FTIR characterizations have shown the formation (in the reaction mixture at 50 °C) of very small Pd/PdO clusters that could be the active sites for low-temperature CO oxidation. This is in line with other studies, which report that isolated Pd species evolve to more active clusters after a pre-reduction step, or in situ in the reaction mixture [20,22,23]. Recently, sub-nanometric 2D PdOx rafts stabilized on Pt/CeO₂ SACs, were found to be thermally stable in oxidizing conditions, efficient for the methane oxidation and resistant to water poisoning [13]. On the other hand, Pd/CeO₂ SACs seem to be not active for the oxidation of propane, which is more difficult to oxidize than CO and is thought to behave differently than methane on Pd catalysts. According to Jeong et al. [23], the propane conversion of a Pd/CeO₂ SAC is negligible up to 350 °C in an oxidizing reaction mixture, suggesting that isolated Pd species do not form clusters in these operating conditions. On the contrary, some studies report the formation of a non-catalytically active CePdOx solid solution in propane/oxygen reaction mixture [24,25]. Interestingly, a very recent study [26] has shown that Pd cations can be also fully dispersed and stabilized on Pr-doped ceria (CP). Pr is a highly reducible element with two Pr³⁺ and Pr⁴⁺ valence states which can

co-exist in oxidizing conditions, leading to the stabilization of oxygen vacancies in ceria. Deng et al. [26] proposed that the better catalytic performances for CO oxidation observed on Pd/CP SACs with respect to Pd/CeO₂ SAC should be linked to oxygen vacancies in the vicinity of in situ-formed Pd clusters. We have recently shown that the concentration of oxygen vacancies in cerium–zirconium–praseodymium (CZP) mixed oxides can be tuned by the quantity of stabilized Pr³⁺ cations which depend both on the preparation method and the composition [27]. For instance, we found that a grinding step can double this Pr³⁺ concentration, resulting in a strong enhancement of the low-temperature reducibility, bulk oxygen mobility and catalytic activity for propane deep oxidation of Pr-rich CZP oxides such as Ce_{0.45}Zr_{0.10}Pr_{0.45}O_{2-x} (CZP45). In the present study, the impact of this highly reducible CZP45 support on the catalytic activity of Pd has been investigated for both CO and propane oxidation. Two CZP45 mixed oxides with the same composition (Ce_{0.45}Zr_{0.10}Pr_{0.45}O_{2-x}) were prepared using a co-precipitation method described in a previous paper [28]. Two variants of this preparation method have led to the synthesis of two materials with different specific surface areas (SSAs), denoted as CZP45-LS and CZP45-HS for low and high SSAs, respectively. A low loading (< 0.2 wt.%) of Pd was impregnated on these oxides to finely disperse Pd. The final catalysts are called Pd-LS and Pd-HS (Table 1), corresponding to Pd supported on CZP45-LS and CZP45-HS, respectively. We follow standard light-off protocols to investigate the impact of a pre-reduction step of the catalysts on the catalytic activity. Temperature programmed reduction (TPR) with H₂ and propane, scanning transmission electron microscopy (STEM) and CO-FTIR (Fourier transform infrared spectroscopy) experiments were performed to unravel the Pd/CZP45 interaction.

Table 1. Catalysts characterization by means of N₂-physisorption, XRD and elemental analysis.

Catalysts	Composition	Pd wt.% ^a	Pd $\mu\text{mol/g}$	SSA (m ² /g)	Pore Volume (cm ³ /g)	Lattice Parameter (Å)	Average Crystal Size (nm) ^b
Pd-LS	Pd/Ce _{0.45} Zr _{0.10} Pr _{0.45} O _{2-x}	0.17	16	6	0.016	5.409	11.6 ± 0.5
Pd-HS	Pd/Ce _{0.45} Zr _{0.10} Pr _{0.45} O _{2-x}	0.14	13	27	0.093	5.398	8.1 ± 0.4

^a determined by ICP-OES analysis, ^b calculated using the Scherrer's equation.

2. Results and Discussion

2.1. Structural and Textural Properties

Diffractograms of Pd-HS and Pd-LS confirm the fluorite structure (SG: Fm-3m) of the two CZP45 supports (Figure 1). No characteristic peak of PdO (JCPDS data (41-1107) [29] or metallic Pd (JCPDS 05-0681) [26] has been detected due to the extremely low Pd loading and a good Pd dispersion. The SSA of Pd-HS is more than 3 times larger than that of Pd-LS (Table 1), in agreement with SSAs of Pd-free supports [28]. The crystal size of Pd-HS, estimated from the Scherrer's equation on the more intense diffraction peak (111), is only slightly lower than that of Pd-LS. This indicates that the highest SSA of Pd-HS can be mainly attributed to a larger intergranular porosity in line with porous volumes (Table 1).

The lattice parameters (Table 1) of the two mixed oxides are lower than those measured in the bare oxides [28]. This suggests a decrease in the rate of stabilized Pr³⁺ (1.12 Å instead of 0.97 Å for Pr⁴⁺) in the two oxides, as probably due to the higher calcination temperature used in the present study (800 °C vs. 700 °C). The lattice parameter of Pd-LS is only slightly higher than that of Pd-HS (Table 1), indicating a similar concentration of Pr³⁺. HAADF-STEM coupled with EDX analysis was used to observe the nanostructure of the two catalysts before and after reduction.

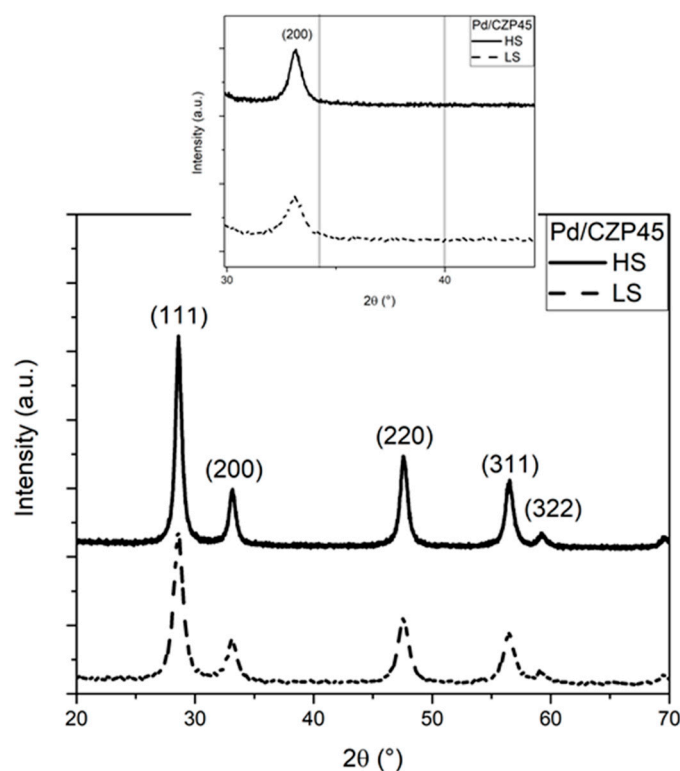


Figure 1. X-Ray diffractogram of Pd-HS and Pd-LS. The insert is a zoom in the 2θ range of the main diffraction peaks of Pd and PdO (solid lines).

Figure S1 (see Supporting Information) displays representative STEM images of Pd-HS after the initial calcination step. Figure S1a,b confirm the fluorite structure of the crystallites according to the distance between atomic columns of Ce/Pr and O. Nanometric crystallites are indeed non-spherical. EDX mappings (Figure S1d,e,f) evidence a homogeneous distribution of the different elements inside the crystallites. However, it was not possible to detect PdO NPs or clusters, suggesting a high Pd dispersion. Similar conclusions can be drawn for Pd-LS (not shown). Please note that the contrast between Pd and ceria is quite small due to the lowest atomic number of Pd. Furthermore, theoretical interplanar distances of PdO and CeO₂ are very close, making the detection of a PdO cluster on ceria very difficult.

STEM images and the corresponding EDX mapping of Pd-HS after reduction, either in H₂ (Figure S2) or in CO (Figure S3), do not clearly detect the presence of Pd clusters, suggesting that Pd is highly dispersed on the support even after a reduction step. Nevertheless, few Pd NPs in the size range 2–3 nm can be observed after a reduction step. Figure 2 gives representative STEM micrographs of Pd NPs formed after a reduction in H₂ (Figure 2a) and in CO (Figure 2b), as confirmed by EDX analysis (bottom insets). The crystal structure of these NPs has been obtained from the fast Fourier transform (FFT). The two diffractograms can be indexed with a cubic Pd structure (JCPDS-03-065-6174) with a lattice parameter of 0.3887 nm. These results demonstrate that metallic Pd NPs have been formed during a reduction step at 500 °C. Only a few NPs were observed, probably due to the low Pd loading and the bad contrast. After a reduction in H₂, Pd NPs seem to be hemispherical, while after a CO reduction, they appear more faceted.

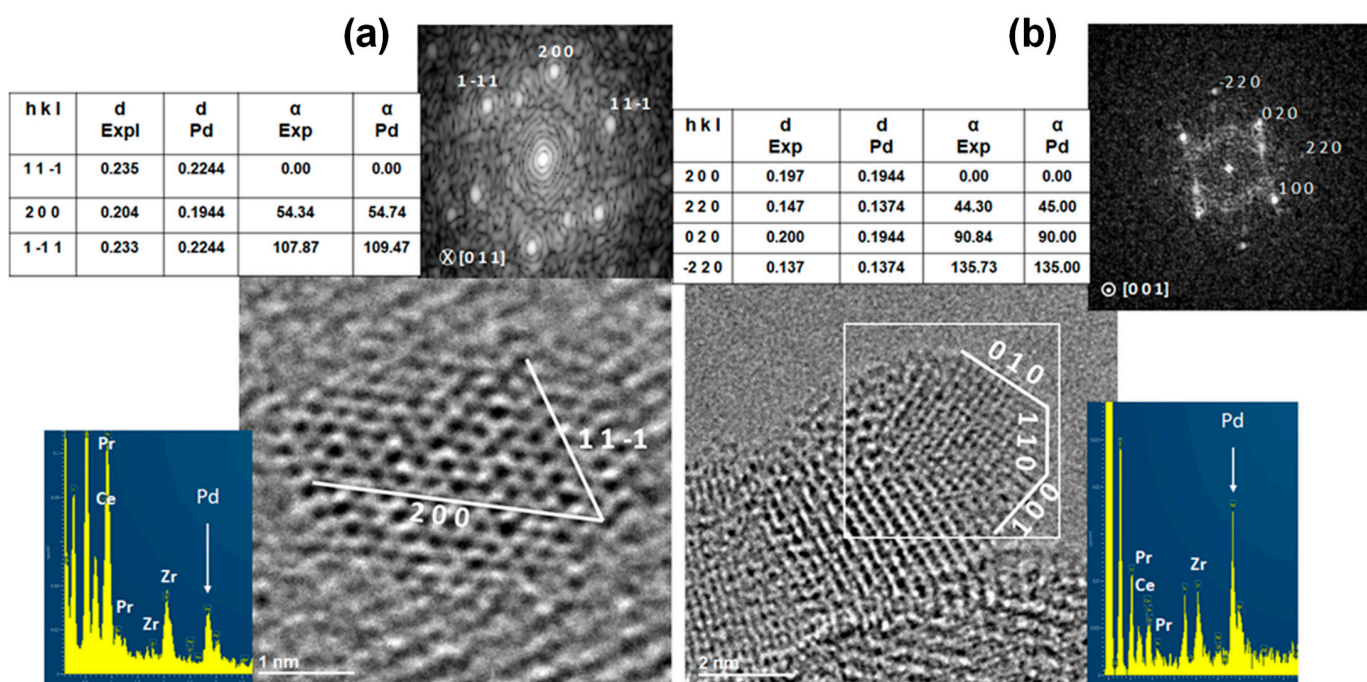


Figure 2. Representative HAADF-STEM micrographs of Pd clusters observed on Pd-HS after a reduction step at 500 °C for 1 h in (a) 100 vol% H₂ and (b) 1 vol% CO/He. The insets are the corresponding FFT (fast Fourier transform) patterns and EDX spectra.

2.2. Reducibility

Figure 3 shows H₂-TPR profiles of Pd-HS and Pd-LS. The two successive TPR experiments are denoted HS1/HS2 and LS1/LS2. The second TPR was run after a redox sequence at 500 °C (1 h in 5 vol% H₂/He and 1 h of re-oxidation in 5 vol% O₂/He) as described in the experimental part. The overall H₂ consumption during LS1 and HS1 far exceeds the theoretical reduction of PdO into Pd (16 μ mol/g for LS1 and 13.1 μ mol/g for HS1), reaching a similar value for both catalysts (Table 2). Their TPR profiles display a non-symmetrical H₂ consumption peak centered at 304 °C and 360 °C, for Pd-HS and Pd-LS, respectively. The reduction of both catalysts starts from around 90 °C and then slowly and gradually grows up to 170 °C on Pd-HS and 250 °C on Pd-LS. According to the literature, the reduction of bulk PdO NPs supported on ceria generally takes place below 100 °C, depending on their size [23,25,30], while small PdOx clusters in close interaction with the support or Pd²⁺ incorporated into ceria such as in Pd-O-Ce bonds [31] are reduced at higher temperatures. Therefore, the two catalysts after the initial calcination step seem to predominantly contain very small PdOx species strongly interacting with CZP45. Furthermore, the reduction of Pd-LS and Pd-HS starts at a higher temperature than that of Pd/CeO₂ catalyst, in which Pd²⁺ cations were incorporated in the fluorite structure [31], suggesting that Pd is mainly dispersed as isolated Pd²⁺ cations on CZP45. The slow initial growth of the reduction at low temperature could correspond to the formation of small Pd clusters by the cleavage of Pd-O-Ce bonds, a prerequisite to trigger the support reduction via the H₂ spillover. A highest SSA promotes the H₂ spillover, explaining the shift to low temperatures of the main reduction peak of Pd-HS compared to Pd-LS. We also notice that the addition of Pd on CPZ45 shifts TPR curves to lower temperatures, confirming the key role of Pd, even at very low loading, in the H₂ chemisorption.

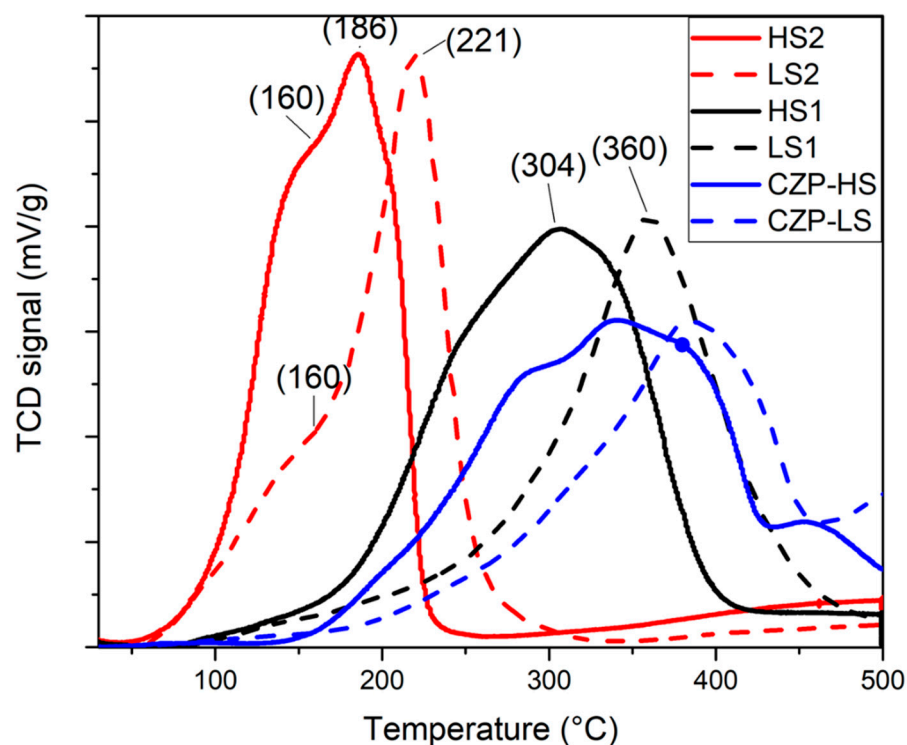


Figure 3. H₂-TPR profiles for Pd-HS, Pd-LS and their bare CZP45 supports.

Table 2. H₂ consumption during H₂-TPR and Pr⁴⁺/Pr³⁺ ratios.

Catalysts	First TPR (LS1 and HS1)		Second TPR (LS2 and HS2)
	H ₂ Uptake (μmol/g) T < 500 °C	H ₂ Uptake (μmol/g) T < 500 °C	Estimation of Initial Pr ⁴⁺ /Pr ³⁺
Pd-HS	1509	1150	81/19
Pd-LS	1472	1105	78/22

The second run of TPR (LS2 and HS2) is different from the first one, showing that the two catalysts have not returned to their initial state after the redox sequence at 500 °C. For both catalysts, the reduction is shifted to low temperature (main peaks centered at 186 °C and 221 °C for Pd-HS and Pd-LS) with a significant increase in the low temperature contribution, as evidenced by a shoulder at around 160 °C for both catalysts. These results demonstrate that Pd NPs formed during the first TPR were not fully re-dispersed as isolated Pd²⁺ cations during the re-oxidation step at 500 °C. Furthermore, the overall H₂ consumption is ca. 25% lower than during the first TPR run (Table 2). This could be due to a less efficient H₂ spillover linked with a smaller Pd/CZP interface and/or an incomplete re-oxidation of the catalyst at 500 °C. The reduction of both samples is taking place below 300 °C. According to the literature [27], one can assume that only Pr⁴⁺ cations are reduced in this low-temperature range. Considering this hypothesis, the overall H₂ consumption below 300 °C would correspond to the reduction of around 80% of Pr atoms in the mixed oxides, suggesting an initial stabilized Pr³⁺ rate near 20% (Table 2).

In summary, TPR experiments suggest that, after the initial calcination step, both catalysts mainly contain isolated Pd²⁺ cations strongly bonded to the support, while the redox sequence at 500 °C triggers the formation of small PdO clusters.

2.3. Lattice Oxygen Reactivity

We used C_3H_8 -TPR experiments to probe the reactivity of oxygen species contained in the catalysts to oxidize propane. Oxygen is stored either in PdO NPs or, mainly, in CZP45 mixed oxides. We have recently shown that lattice mobile oxygen species in CZP45 can oxidize propane into CO_2 from 270 °C during similar C_3H_8 -TPR experiments [28]. As for H_2 -TPR, two successive C_3H_8 -TPR experiments were performed, denoted HS1/HS2 and LS1/LS2. The second TPR was run after a redox sequence at 500 °C (1 h in 5 vol% H_2 /He and 1 h of re-oxidation in 5 vol% O_2 /He).

After the pre-treatment in oxygen at 500 °C, the CO_2 production starts from 225 °C and 250 °C for Pd-HS and Pd-LS, respectively (Figure 4). These temperatures are slightly lower than those observed on bare supports [28]. CO_2 production profiles are composed of two peaks, a small one at low temperatures (centered at around 250–300 °C) and a predominant one centered in the range 370–400 °C. The low-temperature peak should correspond to the propane oxidation with chemisorbed oxygen on the catalysts surface. It is more intense on Pd-HS since its SSA is much higher. Furthermore, the temperature range of this peak coincides with the onset temperature of the oxygen desorption from CZP45 [28]. The high-temperature peaks are linked to the propane oxidation by bulk oxygen species of the mixed oxides. Above 350 °C, an important production of CO on both catalysts (Figure S4) was also observed, suggesting that, at this temperature, the concentration of available lattice oxygen is no more sufficient to deeply oxidize propane. The consumption of lattice oxygen by propane is counter-balanced by the reduction of Pr^{4+} and to a lesser extent of Ce^{4+} above 400 °C.

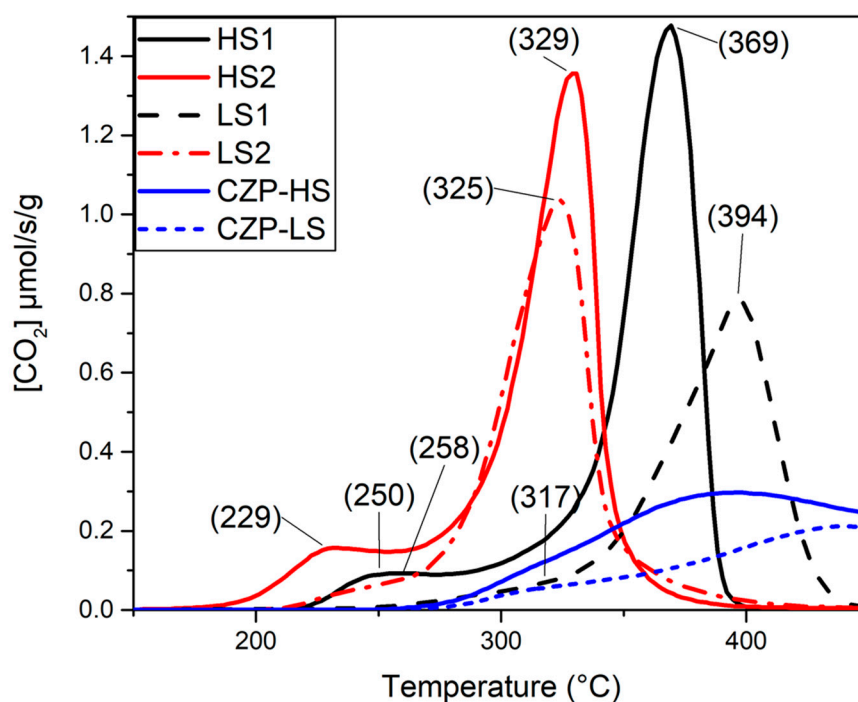


Figure 4. C_3H_8 -TPR profiles for Pd-HS, Pd-LS and their bare supports.

Compared to bare supports, CO_2 production peaks are narrower and shifted to low temperature (Figure 4). A possible assumption is that propane, similarly to H_2 , could cleave Pd-O-Ce bonds (from 225 °C instead of 90 °C in H_2) to form Pd NPs and then accelerate the process. As observed during H_2 -TPR, the dynamic formation of Pd NPs seems to be less efficient on Pd-LS, explaining the higher temperature of the peak (Table 2). After the redox sequence at 500 °C, C_3H_8 -TPR profiles are shifted to lower temperatures (Figure 4 and Table 3) similarly to H_2 -TPR. This is due to the formation of Pd NPs during the reduction step in H_2 at 500 °C which are not fully re-dispersed but re-oxidized during

the re-oxidation phase. These PdO NPs promote the propane adsorption and its oxidation with chemisorbed and lattice oxygen species. Low-temperature peaks correspond to low surface concentrations of oxygen (Table 3), relevant to the oxidation of propane with chemisorbed oxygen on the catalysts surface, considering a mean oxygen surface density of $21.7 \mu\text{mol O}\cdot\text{m}^{-2}$ in ceria-based oxides [32]. The preponderant CO_2 production peak is taking place at the same temperature on both catalysts, indicating that the redox sequence has triggered the formation of similar size-range and concentration of PdO NPs. The overall CO_2 productions are similar to those measured during the first TPR run (Table 3). The two catalysts are also producing CO above 350°C (Figure S4) but with a slightly lower concentration. Considering the overall production of CO_2 and CO at 500°C , 57% and 66% of Pr^{4+} cations were reduced into Pr^{3+} in Pd-LS and Pd-HS, respectively. As expected, the reduction in a propane feed is less pronounced than in H_2 (Table 3). Pd-LS exhibits a lower surface/volume ratio than Pd-HS, explaining that less Pr^{4+} cations are affected by the reduction since they are probably too far from the surface.

Table 3. Main characteristics of C_3H_8 -TPR experiments.

Catalysts	After Oxidation (LS1, HS1)		After a Redox Sequence (LS2, HS2)			
	Low/High Temperature Peak/ $^\circ\text{C}$	$\text{CO}_2 \mu\text{mol/g}$	Low/High Temperature Peak/ $^\circ\text{C}$	$\text{CO}_2 \mu\text{mol/g}$	1st Peak $\mu\text{mol O/m}^{-2}$	CO $\mu\text{mol/g}$
Pd-HS	250/369	309	229/328	312	2.9	347
Pd-LS	317/394	231	258/329	254	4.9	288
CZP45-HS *	-	368				
CZP45-LS *	-	210				

* Data from [28] measured during similar C_3H_8 -TPR up to 600°C .

2.4. Probing Pd Sites Using CO

CO adsorption at RT on Pd-HS was followed by FTIR spectroscopy to obtain further insights into the Pd sites. The catalyst was exposed to only 1 Torr of CO (1.3 mbar) for 1 min to limit a possible reduction and/or rearrangement. Due its low SSA, it was not possible to prepare a thin pellet with Pd-LS.

After the initial calcination at 600°C , the CO adsorption on the catalyst only produces a very weak band at 2138 cm^{-1} (Figure 5a). According to the literature [21,33,34], this band could be attributed to CO linearly adsorbed on Pd^{2+} , i.e., a Pd single atom bound to CeO_2 via two bridged oxygens. More likely, this is also the typical feature of physisorbed CO on the support [35]. Nevertheless, this result indicates that there are no metallic or cationic sites available for the carbon monoxide chemisorption in these conditions. The reduction at 500°C in H_2 strongly modifies the FTIR spectrum of CO adsorption (Figure 5b). Broad, weak, but well defined bands appear below 2000 cm^{-1} , which are generally assigned to CO adsorption on metallic Pd NPs [34]. For instance, bands at 1947 cm^{-1} and 1860 cm^{-1} are attributed to bridged species ($\text{Pd}^0\text{-CO-Pd}^0$) on the Pd(100) crystal planes and triply bridged over Pd(111) planes [36–39], respectively. These results confirm that the reduction step at 500°C triggers the formation of Pd NPs on CZP45, as shown by STEM. The FTIR spectrum also contains a band at 2057 cm^{-1} , attributed to linear CO adsorbed on low coordinated Pd atoms on Pd(111) facet edge [37,40]. The band at 2174 cm^{-1} is assigned to linear CO adsorbed on unsaturated Ce^{4+} [36,41] cations formed during the reduction step.

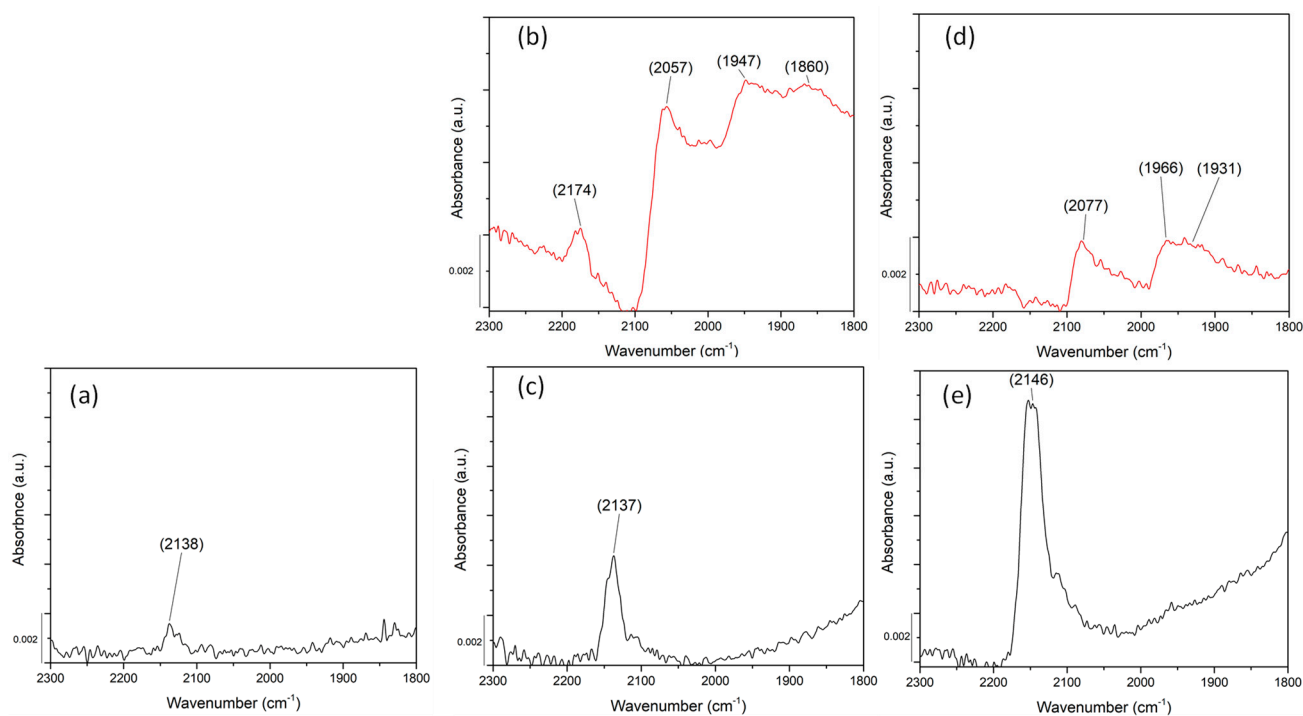


Figure 5. FTIR spectra of Pd-HS after different pre-treatments: (a) after two successive oxidation steps in O₂ at 600 °C for 30 min each, (b) after a reduction in H₂ at 500 °C for 1 h, (c) after a re-oxidation step at 600 °C for 1 h, (d) after two successive reduction steps in CO at 500 °C for 30 min each and (e) after a re-oxidation step at 500 °C in O₂. The spectrum of gaseous CO was subtracted. (a, b, c, d: 1 Torr CO. e: 1.46 Torr CO).

After a re-oxidation at 600 °C, the spectrum (Figure 5c) is similar to that of the fresh sample (Figure 5a), suggesting that Pd NPs formed during the reduction step were re-oxidized atoms at 600 °C in O₂. The band at 2138 cm⁻¹ is even more intense than in Figure 5a. However, a broad band below 2000 cm⁻¹ indicates that some metallic NPs are still present, meaning that some NPs were not re-oxidized, in agreement with TPR results.

The sample was also reduced in CO at 500 °C for 1 h (Figure 5d). As expected, the band at 2138 cm⁻¹ has disappeared while bands characteristic of metallic Pd NP appear, demonstrating the formation of Pd NPs during the CO reduction step. The band at 2077 cm⁻¹ is relative to linear CO adsorbed on low coordinated Pd atoms such as ones located on terraces of Pd clusters [37]. The shift of the linearly coordinated carbonyls to higher wavenumbers upon increasing the reduction temperature indicates that the initial low-coordinated Pd structure collapses, extending the number of coupled $\nu(\text{CO})$ vibrators. Therefore, the $\nu(\text{CO})$ wavenumber of on-top CO species increases [40]. The band at 1966 and 1931 cm⁻¹ could be attributed to CO bridged on two Pd⁰ (Pd⁰-CO-Pd⁰) on (100) and (111) planes, respectively [40]. The reducing agent (either H₂ or CO) during the reduction step impacts the size and nanostructure of formed Pd⁰ NPs, as witnessed by the differences in the bands in FTIR spectra below 2000 cm⁻¹ (Figure 5b,d). After the CO reduction, a final re-oxidation step leads to a similar FTIR spectrum as Figure 5c, confirming the partial the reversibility of the process.

2.5. Catalytic Activity Measurements

Catalytic performances for propane oxidation were measured in lean-burn conditions during four successive light-offs (Figure 6). A reduction step at 500 °C for 1 h either in H₂ (Figure 6a,c,d) or CO (Figure 6b) was performed between the first (LO1) and second light-off (LO2). The catalytic performances of both catalysts during LO1 are poor and comparable to those recorded on bare CZP45 oxides. Figure S5 evidences that the catalytic

performances of Pd-HS and CZP45-HS are similar. In addition, apparent activation energies, E_a , estimated in the low-temperature part of the light-offs (below 20% of conversion) are also in the same range, 81–85 kJ/mol for Pd-HS and Pd-LS, versus 88–90 kJ/mol for CZP45-HS and CZP45-LS [28]. Therefore, the two Pd-based catalysts behave like the bare supports. Another proof of this interpretation is the small production of propene (up to 80 ppm at 450 °C) (Figure S6) and to a lesser extent of ethylene (up to 20 ppm above 550 °C) observed in LO1, which is due to the ability of CZP45 to catalyze the oxidative dehydrogenation of propane, as shown in our previous study [28]. All these results underline that the catalytic activity of isolated Pd^{2+} cations, stabilized after the initial calcination step, is negligible for propane oxidation, in accordance with previous studies [20,23], and coherently with the IR results reported above (Figure 5). This also indicates that the formation of Pd clusters does not occur in a lean propane/oxygen feed. For comparison, the catalytic performances for CO oxidation of both catalysts were also investigated during only one light-off up to 200 °C, recorded after an oxidation step (Figure 7). Both catalysts exhibit great performances for CO oxidation, reaching a full conversion at 150 °C, while Pd-HS is already active at RT. These results corroborate recent studies which have evidenced a high catalytic activity of Pd/CeO₂ SAC [20–23] for CO oxidation, attributed to the operando formation of very small active PdOx clusters. The catalytic activity of Pd-HS is comparable to that of the best Pd/CeO₂ SACs recently reported in the literature (Table 4), despite the smallest SSA of CZP45. Our results highlight that the operando construction of active PdOx clusters in a CO/O₂ reaction mixture can also take place on a Pr-rich CZP mixed oxide.

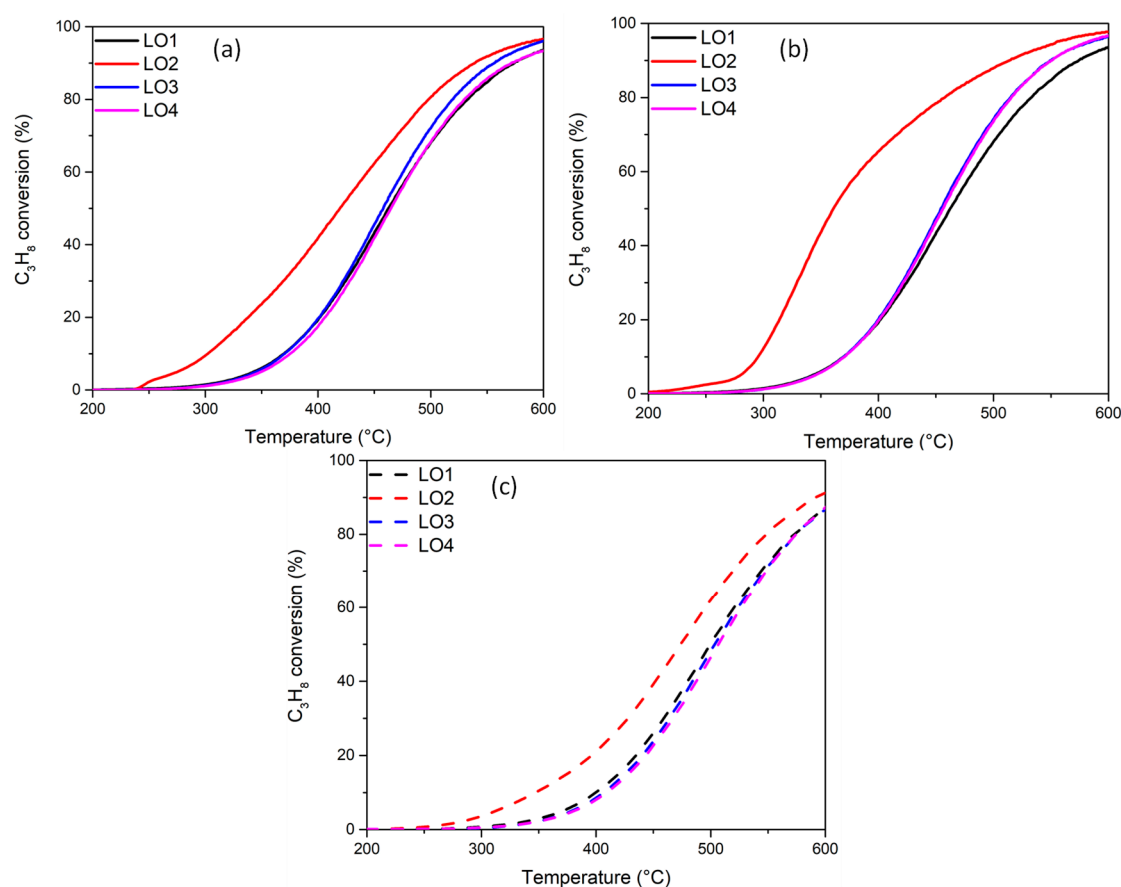


Figure 6. Variation of the propane conversion as a function of the temperature (a) for Pd-HS (reduction step in H_2), (b) for Pd-HS (reduction step in CO), (c) for Pd-LS (reduction step in H_2). Reaction mixture: $\text{C}_3\text{H}_8/\text{O}_2$: 2000 ppm/9 vol%.

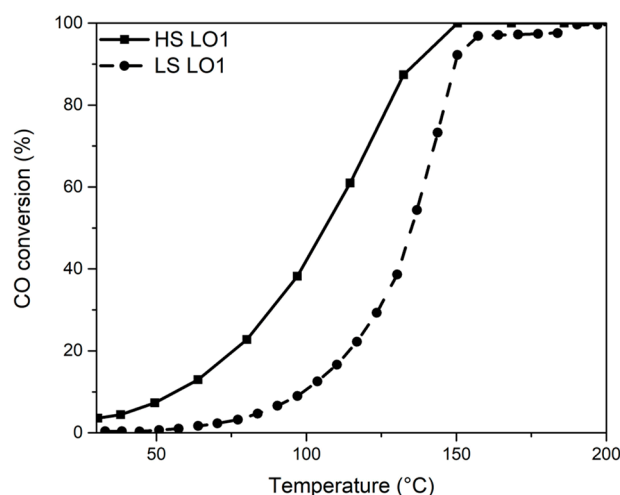


Figure 7. CO conversion for Pd/CZP45-LS and Pd/CZP45-HS. Reaction mixture: CO/O₂: 1910 ppm/9 vol%.

Table 4. Catalytic activity for CO oxidation of Pd-HS and Pd-LS, comparison with the literature data.

Catalysts	Reaction Mixture	GHSV/L·g ⁻¹ ·h ⁻¹	r CO/mol·g ⁻¹ Pd·s ⁻¹ × 10 ⁻⁵			Ref
			50 °C	130 °C	200 °C	
Pd-HS	CO/O ₂ : 1910 ppm/9 vol%	120	12.5	156	196	This study
Pd-LS	CO/O ₂ : 1910 ppm/9 vol%	120	1.02	59	152	This study
1% Pd/CeO ₂ SAC	2 vol% CO/0.1 vol% C ₃ H ₆ /0.1 vol% C ₃ H ₈ /500 ppm NO/ 1.75 vol% O ₂ / 5 vol% H ₂ O	200	-	-	89	[23]
1% Pd/CeO ₂ SAC	CO/O ₂ : 2 vol%/8 vol%	300	34	682	-	[22]
1% Pd/CeO ₂ -Rod	CO/O ₂ : 1 vol%/20 vol%	300	20	-	-	[42]
0.5% Pd/Pr-CeO ₂ 5%	CO/O ₂ : 1 vol%/20 vol%	72	-	32	164	[26]

To improve the catalytic activity for propane combustion, we tried to trigger the formation of Pd clusters with a pre-reduction step. This latter, performed at 500 °C, strongly enhances the catalytic performances for propane oxidation of Pd-HS (Figure 6a,b) and Pd-LS (Figure 6c). For instance, values of T₁₀, corresponding to 10% of conversion of propane which was measured during LO2 (after a reduction step in H₂) is 150–160 °C lower than that observed during LO1. The apparent activation energies also drop after a reduction step (Table 5), suggesting the presence of different active sites before and after reduction. On the opposite, a reduction step has no impact on the catalytic performances of CZP45-HS (Figure S7). A reduction step at 500 °C in H₂ reduces all Pr⁴⁺ cations into Pr³⁺ in CZP45 [28] and then creates a high concentration of oxygen vacancies. Nevertheless, these Pr³⁺ cations are probably rapidly re-oxidized at the introduction of the lean reaction mixture at 200 °C to recover the stabilized concentration of Pr³⁺ in oxidizing conditions near 20%, as estimated by H₂-TPR (Table 2). Therefore, the reduction step mainly impacts the rearrangement of Pd. The strong decrease in the propene and ethylene production during LO2 (Figure S6) confirms this assumption. We assume that metallic Pd NPs, formed during the reduction phase as demonstrated by STEM and CO-FTIR, become the active sites for propane combustion. The beneficial impact of a reduction in CO is more pronounced than in H₂ (Table 5) since the T₅₀ value of Pd-HS drops from 460 °C down to 360 °C (instead

of 419 °C after an H₂ reduction) and the apparent activation energy from 81 to 45 kJ/mol (instead of 63 kJ/mol after a H₂ reduction). This suggests that Pd NPs formed in CO are in greater number and/or more effective than those generated in H₂. The shape of the LO₂ curve also depends on the reducing agent. The propane conversion on Pd-HS, pre-reduced in H₂, slowly and quasi-linearly increases with temperature between 280 and 530 °C, while it abruptly raises between 280 °C and 370 °C after a CO reduction. Furthermore, the production of propene and ethylene is suppressed by the CO reduction (Figure S6). These different behaviors could indicate a higher concentration of Pd active sites after a CO reduction.

Table 5. Catalytic properties for propane oxidation.

Catalysts	LO1				LO2			LO3/LO4		
	T10	T50	Ea kJ/mol	Reduction at 500 °C	T10	T50	Ea kJ/mol	T10	T50	Ea kJ/mol
Pd-HS	370	460	81	100 vol%H ₂	302	419	63	370	458	81
	370	460	81	1 vol% CO	296	360	45	371	455	81
Pd-LS	400	500	85	100 vol%H ₂	347	474	75	406	502	85

The activated state of the reduced catalysts is only temporary, as it is lost in the third LO, which is fairly similar to LO1. The fourth LO (LO4) is also comparable to LO1 and LO3, highlighting a stable state of the two catalysts. Xiong et al. [7] have reported similar results on a Pd/Al₂O₃ catalyst (2 wt.% Pd) and have concluded that metallic Pd obtained after reduction is more active than PdO for propane oxidation. Metallic Pd NPs are slowly oxidized under the reaction mixture, explaining the loss in activity. The situation is more complex in the present study, since the reduction step also triggers the formation of Pd NPs, while a partial redispersion of these NPs may occur in the reaction mixture during light-offs up to 600 °C. To obtain further insight in the re-redispersion, three successive light-offs up to 360 °C and 400 °C were performed on Pd-HS and Pd-LS, respectively, instead of 600 °C in previous experiments. A reduction in H₂ for 1 h at 500 °C was conducted in between LO1 and LO3. Figure S8 confirms the better performances of the two reduced catalysts (LO2). Very interestingly, the catalytic properties during the third LO (LO3) are intermediate between those of LO1 and LO2, demonstrating that the activated state of the reduced catalysts partially persists during LO3. This demonstrates that the redispersion of Pd NPs is thermally activated and can take place below 400 °C, even if it is more efficient at 600 °C. Isothermal experiments were run at 400 °C on a reduced Pd-LS catalyst (500 °C 1 h H₂) in a lean reaction mixture and a rich one (Figure 8a). Similar isothermal experiments were performed at 360 °C on a pre-reduced Pd-HS (Figure S9a). On Pd-LS, the intrinsic catalytic rate is around 235 nmol/s/m² and constant with time in a rich mixture (C₃H₈/O₂ = 2000 ppm/4485 ppm), demonstrating that active Pd NPs formed in the pre-reduction phase are stable at 400 °C in these specific operating conditions. The same conclusion can be drawn at 360 °C on Pd-HS (Figure S9a). In a lean mixture, corresponding to the one used during light-offs (Figure 6), the initial rate is a little bit lower on Pd-LS, compared to that recorded in the rich atmosphere, and rapidly decays with time to reach around 85 nmol/s/m² after 20 min, i.e., the same value recorded in LO1. A similar trend is observed at 360 °C on Pd-HS (Figure S9b). This indicates that the redispersion of Pd NPs at 360 °C is already fast, as 20 min seem to be sufficient to fully recover the activity before reduction. The redispersion is most probably boosted by the high bulk mobility of CZP45. We have also investigated the impact of the propane concentration on the deactivation at 360 °C and 400 °C for Pd-HS (Figure S9b) and Pd-LS (Figure 8b), respectively. For both catalysts, the initial catalytic rate increases with the propane concentration. The reaction order in

propane, considering the initial rates, was estimated to be around +0.6, confirming that the rate-determining step is the activation of propane. The deactivation does not seem to depend on the propane concentration in these operating conditions (high excess of oxygen).

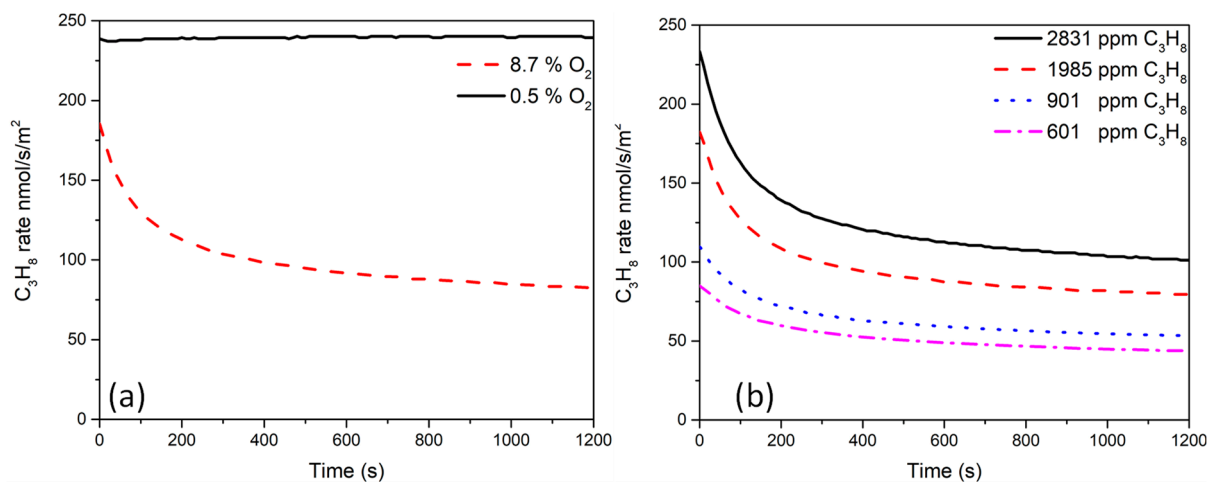


Figure 8. Variation of propane conversion as a function of time for Pd/CZP45-LS at 400 °C (a) for two different oxygen concentrations using 1985 ± 9 ppm of C₃H₈ and (b) for different C₃H₈ concentrations using $8.7\% \pm 0.44\%$ of O₂.

Table 6 compares the catalytic activity for propane oxidation of Pd-LS and Pd-HS after a reduction step with data reported in the literature for Pd/CeO₂ and Pd/Al₂O₃ catalysts. Pd-HS outperforms all these catalysts. For instance, at 320 °C and 350 °C, the catalytic activity of Pd-HS is 5 to 6 times higher than that of a fresh Pd/Al₂O₃ catalyst, containing 3 wt.% of Pd, in similar operating conditions. The activity of Pd-LS is similar to that of Pd/CZ (ceria–zirconia) and Pd/GDC (gadolinia-doped ceria) catalysts after a similar reduction step despite a much lower SSA (34 and 52 m²·g⁻¹ for Pd/GDC and Pd/CZ, respectively). This underlines the outstanding catalytic activity of Pd-LS and Pd-HS catalysts for propane oxidation after a reduction step. The activation of propane on finely dispersed Pd NPs, formed during the reduction step, coupled with the very high oxygen mobility of CZP45, explains the good performances of these materials. However, the re-oxidation of Pd promoted by the fast oxygen mobility of the support rapidly deactivates the catalysts in lean conditions. Nevertheless, the optimized state of Pd/CZP45 catalysts can be maintained in a rich reaction mixture. For instance, the catalytic activity of Pd-HS reaches 0.96 mmol·g⁻¹ Pd·s⁻¹ at 360 °C (Figure S9). For comparison, the catalytic activity of a Pd/GDC catalyst (1 wt.% Pd, SSA = 34 m²·g⁻¹), pre-reduced at 500 °C in H₂ for 1 h, is around 3 times lower (0.35 mmol·g⁻¹ Pd·s⁻¹) at 360 °C in a stoichiometric propane/O₂ feed.

Table 6. Catalytic activity for C₃H₈ oxidation and comparison with the literature data.

Catalysts	Reaction Mixture	GHSV/L·g ⁻¹ ·h ⁻¹	Pre-Treatment	r C ₃ H ₈ /mol·g ⁻¹ Pd·s ⁻¹ × 10 ⁻⁵		Ref
				320 °C	350 °C	
Pd-HS	C ₃ H ₈ /O ₂ : 2000 ppm/9 vol%	120	CO reduction, 500 °C, 1 h	46	84	This study
Pd-HS	C ₃ H ₈ /O ₂ : 2000 ppm/9 vol%	120	H ₂ reduction, 500 °C, 1 h	28	45	This study
Pd-LS	C ₃ H ₈ /O ₂ : 2000 ppm/9 vol%	120	H ₂ reduction, 500 °C, 1 h	9.7	16	This study
0.3% Pd/CeO ₂	C ₃ H ₈ /O ₂ : 2000 ppm/2 vol%	30	Ar, 200 °C, 0.5 h	12	22	[20]
0.3% Pd/CeO ₂ SAC	C ₃ H ₈ /O ₂ : 2000 ppm/2 vol%	30	Ar, 200 °C, 0.5 h	3.8	9	[20]
1% Pd/CeO ₂ -O (octahedron)	C ₃ H ₈ /O ₂ : 2000 ppm/2 vol%	300	H ₂ reduction, 200 °C, 0.5 h	10	-	[42]
1% Pd/CeO ₂ -cube	C ₃ H ₈ /O ₂ : 2000 ppm/2 vol%	300	H ₂ reduction, 200 °C, 0.5 h	1.6	-	[42]
1% Pd/CeO ₂ -Rod	C ₃ H ₈ /O ₂ : 2000 ppm/2 vol%	300	H ₂ reduction, 200 °C, 0.5 h	0.8	-	[42]
2% Pd/CeZr/Al ₂ O ₃	C ₃ H ₈ /O ₂ : 3000 ppm/3 vol% O ₂	30	Calcination 900 °C, 2h	0.7	2.9	[43]
2% Pd/Ce-Zr- Y/Al ₂ O ₃	C ₃ H ₈ /O ₂ : 3000 ppm/3 vol%	30	Calcination 900 °C, 2h	0.7	2.9	[43]
3% Pd/Al ₂ O ₃	C ₃ H ₈ /O ₂ : 1750 ppm/2 vol% O ₂	300	N ₂ , 500 °C, 0.5 h	9.9	14	[44]
1.1% Pd/Al ₂ O ₃	C ₃ H ₈ /O ₂ /H ₂ O 500 ppm/5 vol%/ 5 vol%	768	H ₂ reduction, 250 °C, 0.5 h	1.1	1.9	[7]
0.5% Pd/CeO ₂	C ₃ H ₈ /O ₂ : 5000 ppm/5 vol%	15	Calcination 500 °C, 4h	3.4	5.7	[45]
1% Pd/GDC (Ce _{0.8} Gd _{0.2} O ₂)	C ₃ H ₈ /O ₂ : 2000 ppm/1 vol%	360	H ₂ reduction, 500 °C, 1 h	12.5	28	[25]
1% Pd/CZ (Ce _{0.62} Zr _{0.38} O ₂)	C ₃ H ₈ /O ₂ : 2000 ppm/1 vol%	360	H ₂ reduction, 500 °C, 1 h	10	18	[25]

3. Materials and Methods

3.1. Synthesis

Two CZP45 oxides were prepared using a co-precipitation method described in a previous paper [28], which was modified to achieve different SSAs. These oxides were ground with a mixer-mill (MM-200-Retsch) in a ball-mortar containing two zirconia balls of 5 mm diameter at 10 Hz for 6 h. This grinding step was found to enhance the stabilization of Pr³⁺ cations in CZP mixed oxides [28]. A low loading of Pd (<0.2 wt.%) was then dispersed on these two oxides by wet impregnation in order to combine a high dispersion and a low price by using a small amount of Pd. tetraaminepalladium (II) nitrate (Pd(NH₃)₄(NO₃)₂ Sigma Aldrich, 10 wt.% in H₂O, purity 99.99%) was used as Pd precursor, dissolved in 5 mL of water and mixed with the mixed oxides powder. The obtained mixture was stirred under vacuum for 1 h in a rotavapor (150 rpm) and then evaporated by progressively heating until 90 °C. The achieved powder was dried overnight at 80 °C in a furnace, then calcined

under flowing air for 8 h at 800 °C. According to Jiang et al. [22], this high-temperature calcination should promote the stabilization of isolated Pd²⁺ on the ceria surface.

3.2. Catalyst Characterizations

The Pd content in the catalysts was quantified by inductively coupled plasma emission spectroscopy (ICP-OES, Activa spectrometer from Horiba, EDISON, USA), N₂ physisorption at −196 °C was performed after a degassing step under vacuum (10^{−5} bar) at 300 °C overnight. The SSA was calculated according to the Brunauer–Emmett–Teller (BET, Tristar instrument from Micromeritics, USA) method. The X-ray diffraction (XRD, Bruker D8 Advance A25, Germany) pattern of the catalysts was recorded at room temperature using an X-ray powder diffractometer with the CuKα_{1,2} radiation ($\lambda = 0.1518$ nm) in a wide range of Bragg angles 2θ (20–80 °) with a step of 0.020 ° and a counting time of 100 s. The lattice parameter was calculated using Vegard's law and the crystal size using Scherrer's equation.

H₂-temperature programmed reduction TPR experiments were performed on a Thermoquest TPDRO 1100 (Thermo Electron Corporation, Waltham, MA, USA) analyzer equipped with a thermal conductivity detector (TCD). First, the catalyst (around 100 mg) was pre-treated at 500 °C (10 °C min^{−1}) for 1 h with 40 mL.min^{−1} of 5 vol% O₂/He to clean the surface and then cooled down to room temperature still under O₂. After an He purge, the H₂ consumption at room temperature (RT) was measured by quantifying the consumption during two successive introductions of H₂ (40 mL min^{−1} of 5 vol% H₂/He) with a 10 min purge under He in between. The difference in the two H₂ profiles gave the H₂ consumption due to the reduction of the sample at RT. Then, a first TPR was recorded during a heating ramp (10 °C min^{−1}) up to 500 °C followed by a plateau of 1 h in 40 mL min^{−1} of 5 vol% H₂/He. After an He rich purge, the same cycle was repeated to perform a second TPR after a re-oxidation at 500 °C for 1 h.

C₃H₈-TPR analysis were also performed to probe the reactivity of surface and bulk oxygen of the catalysts. Around 100 mg of each sample was pre-treated at 500 °C in O₂ (5 vol%) for 1 h to clean and oxidize the surface. Then, it was cooled down to RT under O₂ (5 vol%). C₃H₈-TPD experiments were operated with 2000 ppm C₃H₈ in He (12 L h^{−1}) up to 600 °C (10 °C min^{−1}). C₃H₈-TPD after an oxidizing pre-treatment is named "oxidized". A second C₃H₈-TPD experiment was carried out after a redox pre-treatment and named "redox". This latter took place at 500 °C and consisted of an oxidation step for 1 h under 5% O₂, followed by a reduction in pure H₂ for 1 h and a re-oxidation phase in 5 vol% O₂ for 1 h. Analysis of O₂, CO, CO₂, C₂H₄, C₃H₆ and C₃H₈ during C₃H₈-TPR was performed with a micro gas-chromatograph (SRA 3000, France) equipped with two TCD detectors, a molecular sieve and a Porapak Q column. The CO₂ concentration was also recorded by an on-line IR analyzer (Horiba, Japan).

Ex situ scanning transmission electron microscopy (STEM, ThermoScientific™, Waltham, MA, USA) was used to observe Pd nanoparticles with an environmental transmission electron microscope (Ly-ETEM, ThermoScientific™ TITAN ETM G2 80–300 Kv, ThermoScientific™, Waltham, MA, USA) corrected for the aberrations of the objective lens and equipped with energy-dispersed X-ray spectroscopy (EDX). For this purpose, the samples were suspended in ethanol and transferred onto a carbon-covered Cu-grid. Bright Field TEM and Annular Dark Field-STEM (ADF-STEM, ThermoScientific™, Waltham, MA, USA) images were acquired at 300 kV under high vacuum.

Pd sites on Pd-HS were identified by using CO as a probe molecule using in situ IR (Horiba, Japan) measurement. Catalysts (24–28 mg) were pressed (~1 ton.cm^{−2}) into cylindrical thin pellets with a diameter of 16 mm. However, the quantity of species adsorbed on the low SSA Pd-LS catalyst was too low to obtain relevant FTIR spectra (Thermo Scientific Nicole iS50 FTIR spectrometer, Thermo Scientific, Waltham, MA, USA). We focused our efforts on Pd-HS. This latter was pre-treated at 600 °C under pure O₂ (66 mbar) for 20 min, then cooled down to RT still in presence of oxygen and exposed to high vacuum for 15 min to evacuate CO₂ from the IR cell. CO₂ was supposed to come from the decomposition of surface carbonates at 600 °C. The evacuation under vacuum

was performed at RT to avoid any surface reduction that could occur at 600 °C. Oxygen was again introduced (66 mbar) at RT and the pellet was heated up to 600 °C for 20 min for a second oxidation step on a carbonate-free surface, cooling down again in O₂ at RT where the oxygen was removed from the cell under high vacuum. Finally, CO (1.3 mbar) was adsorbed at RT for 1 min and IR spectra were recorded (64 scans). The CO adsorption state was limited to 1 min to avoid a possible reduction and/or rearrangement of the catalyst. After that, a re-oxidation of the same pellet was then performed during two successive treatments at 600 °C in O₂ (66 mbar) of 15 min (carbonate decomposition) and 45 min (oxidation of a carbonate-free surface), respectively. In between these two steps, the catalyst was exposed to high vacuum to remove CO₂. Then, the pellet was cooled down in O₂ to RT, evacuated in high vacuum before the CO adsorption measurement for 1 min.

A similar CO adsorption was performed after a first oxidation step of a fresh pellet at 600 °C for 15 min in O₂ (66 mbar) to desorb carbonates following by a cooling-down at 500 °C still in O₂. At 500 °C, the oxygen was removed under high vacuum and 133 mbar of pure H₂ were introduced for 1 h to reduce the catalyst and then evacuated in high vacuum. After a cooling-down in vacuum at RT, CO was introduced and adsorbed for 1 min and IR spectra recorded. Then, the same pellet was re-oxidized at 600 °C in O₂ (66 mbar) in two steps as initially (15 min/high vacuum/45 min), cooled down in O₂ to RT, where CO was chemisorbed again for 1 min after the evacuation of O₂ in high vacuum. A similar sequence of measurements was performed on a fresh pellet, except that the reduction step occurred in the presence of CO at 500 °C. Two successive reduction steps in 10 mbar of CO for 30 min each were performed with an evacuation in high vacuum in between to remove CO₂ produced by the first reduction phase. The CO adsorption at RT was then analyzed by FTIR. A similar re-oxidation step at 600 °C than after the H₂ reduction was carried out before adsorbing again CO at RT. The signature of CO in the phase gas was systemically subtracted from all FTIR spectra.

3.3. Catalytic Activity Measurement

A mass of ca. 100 mg of each catalyst was placed in a U-shaped quartz reactor equipped with a porous fine-quartz fritted disk. The catalytic performances were measured during successive light-offs (LOs). These latter were performed using a 12 L h⁻¹ total gas flow, yielding a gas hourly space velocity of around 50,000 h⁻¹ and 100 L g_{cat}⁻¹ h⁻¹. An oxidizing pre-treatment at 600 °C in O₂ (5 vol%) for 1 h followed by cooling down in O₂ were systematically performed before the first LO denoted as LO1. After that, the catalyst was reduced in pure H₂ at 500 °C for 1 h for reducing PdO into Pd. The cooling down to 200 °C was performed under the same atmosphere to avoid the Pd re-oxidation. The reactive mixture was introduced at 200 °C after a short He purge. Then, three successive LOs, denoted as LO2, LO3 and LO4, were raised without any treatment in between. For propane combustion, a typical experiment consisted of 4 successive LOs (LO1, LO2, LO3 and LO4) from 200 up to 600 °C using a heating ramp of 4 °C min⁻¹ with a 5 min dwell at the maximal temperature. Four successive LOs from 200 °C until 360 °C and 400 °C for Pd-HS and Pd/-LS, respectively, were performed. The catalytic performance for C₃H₈ combustion was investigated in lean dry condition (1985 ppm C₃H₈, 9 vol% O₂ in He). Water was not introduced in the reaction mixture to clearly highlight the impact of the pre-reduction step.

Isothermal measurements were also performed after a pre-treatment step at 500 °C for 1 h (either in O₂ or in H₂) by varying the partial pressure of propane and O₂ at 360 °C and 400 °C for Pd-HS and Pd/-LS, respectively. It was checked, by varying the overall gas flow, that the propane oxidation was in a chemical regime at 360 °C and 400 °C.

A similar protocol was used for CO oxidation, except that the reaction mixture (1910 ppm CO and 9 vol% O₂ in He) was introduced at RT instead of 200 °C up to 500 °C. Reactants and products were analyzed with the same gas micro-chromatograph and online CO₂ IR analyzer as for C₃H₈-TPD experiments. Reactants were Linde certified standards C₃H₈ in He (8006 ppm), CO in He (4971 ppm) and O₂ (three used concentrations: 1, 5 and

99.995 vol%) that could be further diluted in He (99.995%). The carbon balance closure was found to be below 5 vol% for both CO and propane oxidation. CO₂ was the predominant carbon-based product detected during propane oxidation catalytic tests. However, ethylene and propene were also detected, as discussed in the Results.

4. Conclusions

A small loading of Pd (<0.2 wt.%) was dispersed on Pr-rich CZP mixed oxides (CZP45: Ce_{0.45}Zr_{0.10}Pr_{0.45}O_{2-x}). After the initial calcination at 800 °C, Pd is mainly in the form of fully dispersed isolated cations in strong interaction with CZP45. Their catalytic performances for propane oxidation are similar to those of the bare supports, demonstrating their inactivity. Conversely, as-prepared Pd/CZP45 catalysts are quite efficient for low-temperature CO oxidation, suggesting that isolated Pd cations *operando* evolve to small active PdOx clusters. Pd/CZP45 catalysts were pre-reduced to trigger the formation of Pd nanoparticles and promote the propane oxidation. The finely dispersed Pd nanoparticles, formed during the reduction step, coupled with the very high oxygen mobility of CZP45, lead to outstanding catalytic activity for propane oxidation starting from 250 °C. However, the re-oxidation of Pd nanoparticles and their partial re-dispersion, promoted by the fast oxygen mobility of the mixed oxide, rapidly deactivate the catalysts in lean conditions. For instance, the catalytic activity was found to return to its value before the reduction step in less than 20 min at 360 °C. Additional experiments could be quite interesting to investigate the stability of the catalytic performances below 300 °C. Nevertheless, the optimized state of a pre-reduced Pd/CZP45 catalyst can be maintained in a rich reaction mixture at 400 °C, as encountered in three-way catalytic converters.

Supplementary Materials: The following supporting information can be downloaded at: <https://www.mdpi.com/article/10.3390/catal12080827/s1>, Figure S1: (a,c) Representative HAADF-STEM images of Pd-HS, (b) zoom in the with square of (a) showing atomic columns of Ce and O characteristic of a plan (001) of a CeO₂ fluorite structure, (d–g) EDX mappings of Ce, Pr, Zr and Pd, respectively; Figure S2: TEM image of Pd-HS after reduction in H₂ (500 °C, 1 h, 100 vol% H₂) and EDX mapping of Ce, Pr, Zr and Pd; Figure S3: TEM image of Pd-HS after reduction in CO (500 °C, 1 h, 1 vol% CO) and EDX mapping of Ce, Pr, Zr and Pd; Figure S4: Variation of the CO production as a function of the temperature for (a) Pd-HS and (b) Pd-LS during C₃H₈-TPD experiments; Figure S5: Variation of the propane conversion as a function of the temperature for Pd-HS (catalyst mass = 100 mg) and CZP45-HS (catalyst mass = 90 mg). Reactive mixture: C₃H₈/O₂: 2000 ppm/9 vol%; Figure S6: Secondary products analyzed during propane oxidation experiments on Pd-HS: (a) LO2 after an H₂ reduction and (b) LO2 after a CO reduction; Figure S7: Variation of the propane conversion as a function of the temperature for CZP45-HS (reduction step in H₂.) Reactive mixture: C₃H₈/O₂: 2000 ppm/9 vol%. Catalyst mass = 90 mg; Figure S8: Variation of the propane conversion as a function of the temperature: (a) on Pd-HS up to 360 °C and (b) on Pd-LS up to 400 °C. The reduction step between LO1 and LO2 was performed in H₂; Figure S9: Variation of the intrinsic reaction rate as a function of time for Pd-HS at 360 °C (a) for different oxygen concentrations using 1985 ± 9 ppm of C₃H₈ and (b) for different C₃H₈ concentration using 8.7 vol% of O₂.

Author Contributions: Conceptualization, A.D., M.D. and P.V.; methodology, P.B., A.D., M.D. and P.V.; formal analysis, S.F.; investigation, S.F., R.P., M.A., A.B. and P.B.; resources, A.D., M.D. and P.V.; data curation, P.B., M.A., M.D. and P.V.; writing—original draft preparation, S.F. and P.V.; writing—review and editing, S.G., P.B. and M.D.; supervision, A.D., M.D. and P.V.; project administration, A.D., M.D. and P.V.; funding acquisition, A.D. All authors have read and agreed to the published version of the manuscript.

Funding: This research was funded by The French National Research Agency ‘Agence Nationale de la Recherche’ (ANR), grant number ANR-17-CE08-0022-02.

Data Availability Statement: All data can be obtained from the corresponding author upon reasonable request.

Acknowledgments: The authors thank the CLYM for access to the Ly-E TEM and The French National Research Agency ‘Agence Nationale de la Recherche’ (ANR).

Conflicts of Interest: The authors declare no conflict of interest.

References

1. Farrauto, R.J.; Deeba, M.; Alerasool, S. Gasoline automobile catalysis and its historical journey to cleaner air. *Nat. Catal.* **2019**, *2*, 603–613. [[CrossRef](#)]
2. Au-Yeung, J.; Chen, K.; Bell, A.T.; Iglesia, E. Isotopic studies of methane oxidation pathways on PdO catalysts. *J. Catal.* **1999**, *188*, 132–139. [[CrossRef](#)]
3. Colussi, S.; Trovarelli, A.; Groppi, G.; Llorca, J. The effect of CeO₂ on the dynamics of Pd-PdO transformation over Pd/Al₂O₃ combustion catalysts. *Catal. Commun.* **2007**, *8*, 1263–1266. [[CrossRef](#)]
4. Lott, P.; Dolcet, P.; Casapu, M.; Grunwaldt, J.D.; Deutschmann, O. The effect of prereduction on the performance of Pd/Al₂O₃ and Pd/CeO₂ catalysts during methane oxidation. *Ind. Eng. Chem. Res.* **2019**, *58*, 12561–12570. [[CrossRef](#)]
5. Wang, D.; Gong, J.; Luo, J.; Li, J.; Kamasamudram, K.; Currier, N.; Yezerets, A. Distinct reaction pathways of methane oxidation on different oxidation states over Pd-based three-way catalyst (TWC). *Appl. Catal. A Gen.* **2019**, *572*, 44–50. [[CrossRef](#)]
6. Karinshak, K.A.; Lott, P.; Harold, M.P.; Deutschmann, O. In situ Activation of Bimetallic Pd–Pt Methane Oxidation Catalysts. *ChemCatChem* **2020**, *12*, 3712–3720. [[CrossRef](#)]
7. Xiong, H.; Wiebenga, M.H.; Carrillo, C.; Gaudet, J.R.; Pham, H.N.; Kunwar, D.; Oh, S.H.; Qi, G.; Kim, C.H.; Datye, A.K. Design considerations for low-temperature hydrocarbon oxidation reactions on Pd based catalysts. *Appl. Catal. B Environ.* **2018**, *236*, 436–444. [[CrossRef](#)]
8. Ciuparu, D.; Perkins, E.; Pfefferle, L. In situ DR-FTIR investigation of surface hydroxyls on γ -Al₂O₃ supported PdO catalysts during methane combustion. *Appl. Catal. A Gen.* **2004**, *263*, 145–153. [[CrossRef](#)]
9. Chin, Y.H.; Buda, C.; Neurock, M.; Iglesia, E. Consequences of metal-oxide interconversion for C-H bond activation during CH₄ reactions on Pd catalysts. *J. Am. Chem. Soc.* **2013**, *135*, 15425–15442. [[CrossRef](#)]
10. Goodman, E.D.; Dai, S.; Yang, A.C.; Wrasman, C.J.; Gallo, A.; Bare, S.R.; Hoffman, A.S.; Jaramillo, T.F.; Graham, G.W.; Pan, X.; et al. Uniform Pt/Pd Bimetallic Nanocrystals Demonstrate Platinum Effect on Palladium Methane Combustion Activity and Stability. *ACS Catal.* **2017**, *7*, 4372–4380. [[CrossRef](#)]
11. Nagai, Y.; Hirabayashi, T.; Dohmae, K.; Takagi, N.; Minami, T.; Shinjoh, H.; Matsumoto, S. Sintering inhibition mechanism of platinum supported on ceria-based oxide and Pt-oxide-support interaction. *J. Catal.* **2006**, *242*, 103–109. [[CrossRef](#)]
12. Jones, J.; Xiong, H.; DeLaRiva, A.T.; Peterson, E.J.; Pham, H.; Challa, S.R.; Qi, G.; Oh, S.; Wiebenga, M.H.; Hernández, X.I.P.; et al. Thermally stable single-atom platinum-on-ceria catalysts via atom trapping. *Science* **2016**, *353*, 150–154. [[CrossRef](#)] [[PubMed](#)]
13. Xiong, H.; Kunwar, D.; Jiang, D.; García-Vargas, C.E.; Li, H.; Du, C.; Canning, G.; Pereira-Hernandez, X.I.; Wan, Q.; Lin, S.; et al. Engineering catalyst supports to stabilize PdOx two-dimensional rafts for water-tolerant methane oxidation. *Nat. Catal.* **2021**, *4*, 830–839. [[CrossRef](#)]
14. Reddy, K.P.; Choi, H.; Kim, D.; Choi, M.; Ryoo, R.; Park, J.Y. The facet effect of ceria nanoparticles on platinum dispersion and catalytic activity of methanol partial oxidation. *Chem. Commun.* **2021**, *57*, 7382–7385. [[CrossRef](#)]
15. Yoo, M.; Yu, Y.S.; Ha, H.; Lee, S.; Choi, J.S.; Oh, S.; Kang, E.; Choi, H.; An, H.; Lee, K.S.; et al. A tailored oxide interface creates dense Pt single-atom catalysts with high catalytic activity. *Energy Environ. Sci.* **2020**, *13*, 1231–1239. [[CrossRef](#)]
16. Gänzler, A.M.; Casapu, M.; Maurer, F.; Störmer, H.; Gerthsen, D.; Ferré, G.; Vernoux, P.; Bornmann, B.; Frahm, R.; Murzin, V.; et al. Tuning the Pt/CeO₂ Interface by in Situ Variation of the Pt Particle Size. *ACS Catal.* **2018**, *8*, 4800–4811. [[CrossRef](#)]
17. Ferré, G.; Aouine, M.; Bosselet, F.; Burel, L.; Aires, F.J.C.S.; Geantet, C.; Ntais, S.; Maurer, F.; Casapu, M.; Grunwaldt, J.; et al. Exploiting the dynamic properties of Pt on ceria for low-temperature CO oxidation. *Catal. Sci. Technol.* **2020**, *10*, 3904–3917. [[CrossRef](#)]
18. Colussi, S.; Gayen, A.; Camellone, M.F.; Boaro, M.; Llorca, J.; Fabris, S.; Trovarelli, A. Nanofaceted Pd—O Sites in Pd—Ce Surface Superstructures: Enhanced Activity in Catalytic Combustion of Methane. *Angew. Chem. Int. Ed.* **2009**, *48*, 8481–8484. [[CrossRef](#)]
19. Bruix, A.; Rodriguez, J.A.; Ramirez, P.J.; Senanayake, S.D.; Evans, J.; Park, J.B.; Stacchiola, D.; Liu, P.; Hrbek, J.; Illas, F. A new type of strong metal-support interaction and the production of H₂ through the transformation of water on Pt/CeO₂(111) and Pt/CeO_x/TiO₂(110) catalysts. *J. Am. Chem. Soc.* **2012**, *134*, 8968–8974. [[CrossRef](#)]
20. You, R.; Li, Z.; Cao, T.; Nan, B.; Si, R.; Huang, W. Synthesis in a Glovebox: Utilizing Surface Oxygen Vacancies To Enhance the Atomic Dispersion of Palladium on Ceria for Carbon Monoxide Oxidation and Propane Combustion. *ACS Appl. Nano Mater.* **2018**, *1*, 4988–4997. [[CrossRef](#)]
21. Spezzati, G.; Su, Y.; Hofmann, J.P.; Benavidez, A.D.; DeLaRiva, A.T.; McCabe, J.; Datye, A.K.; Hensen, E.J.M. Atomically dispersed Pd-O species on CeO₂(111) as highly active sites for low-temperature CO oxidation. *ACS Catal.* **2017**, *7*, 6887–6891. [[CrossRef](#)] [[PubMed](#)]
22. Jiang, D.; Wan, G.; García-Vargas, C.E.; Li, L.; Pereira-Hernández, X.I.; Wang, C.; Wang, Y. Elucidation of the Active Sites in Single-Atom Pd₁/CeO₂ Catalysts for Low-Temperature CO Oxidation. *ACS Catal.* **2020**, *10*, 11356–11364. [[CrossRef](#)]
23. Jeong, H.; Kwon, O.; Kim, B.S.; Bae, J.; Shin, S.; Kim, H.E.; Kim, J.; Lee, H. Highly durable metal ensemble catalysts with full dispersion for automotive applications beyond single-atom catalysts. *Nat. Catal.* **2020**, *3*, 368–375. [[CrossRef](#)]
24. Baek, K.; Min, K.; Kim, K.; Ha, Y. Propane combustion over supported Pd catalysts. *Res. Chem. Intermed.* **2010**, *36*, 603–611. [[CrossRef](#)]
25. Lopez-Gonzalez, D.; Couble, J.; Aouine, M.; Massin, L.; Mascunan, P.; Díez-Ramírez, J.; Klotz, M.; Tardivat, C.; Vernoux, P. Effect of the Reduction Step on the Catalytic Performance of Pd–CeMO₂ Based Catalysts (M = Gd, Zr) for Propane Combustion. *Top Catal.* **2016**, *59*, 1638–1650. [[CrossRef](#)]

26. Deng, Y.; Tian, P.; Liu, S.; He, H.; Wang, Y.; Ouyang, L.; Yuan, S. Enhanced catalytic performance of atomically dispersed Pd on Pr-doped CeO₂ nanorod in CO oxidation. *J. Hazard. Mater.* **2021**, *426*, 127793. [CrossRef]
27. Frizon, V.; Bassat, J.M.; Pollet, M.; Durand, E.; Hernandez, J.; Pajot, K.; Vernoux, P.; Demourgues, A. Tuning the Pr Valence State to Design High Oxygen Mobility, Redox and Transport Properties in the CeO₂-ZrO₂-PrO_x Phase Diagram. *J. Phys. Chem. C* **2019**, *123*, 6351–6362. [CrossRef]
28. Fahed, S. Étude Des Oxydes Mixtes Cérium-Zirconium-Praséodyme Pour L'Oxydation Des Composés Imbrûlés Emis Par Les Moteurs à Essence et Diesel. Ph.D. Thesis. 2022. Available online: <https://www.theses.fr/2022NORMC211> (accessed on 7 July 2022).
29. Colussi, S.; Trovarelli, A.; Cristiani, C.; Lietti, L.; Groppi, G. The influence of ceria and other rare earth promoters on palladium-based methane combustion catalysts. *Catal. Today* **2012**, *180*, 124–130. [CrossRef]
30. Luo, M.F.; Hou, Z.Y.; Yuan, X.X.; Zheng, X.M. Characterization study of CeO₂ supported Pd catalyst for low-temperature carbon monoxide oxidation. *Catal. Lett.* **1998**, *50*, 205–209. [CrossRef]
31. Hiley, C.I.; Fisher, J.M.; Thompsett, D.; Kashtiban, R.J.; Sloan, J.; Walton, R.I. Incorporation of square-planar Pd²⁺ in fluorite CeO₂: Hydrothermal preparation, local structure, redox properties and stability. *J. Mater. Chem. A* **2015**, *3*, 13072–13079. [CrossRef]
32. Madier, Y.; Descorme, C.; Le Govic, A.M.; Duprez, D. Oxygen mobility in CeO₂ and CexZr_(1-x)O₂ compounds: Study by CO transient oxidation and ¹⁸O/¹⁶O isotopic exchange. *J. Phys. Chem. B* **1999**, *103*, 10999–11006. [CrossRef]
33. Spezzati, G.; Benavidez, A.D.; DeLaRiva, A.T.; Su, Y.; Hofmann, J.P.; Asahina, S.; Olivier, E.J.; Neethling, J.H.; Miller, J.T.; Datye, A.K.; et al. CO oxidation by Pd supported on CeO₂(100) and CeO₂(111) facets. *Appl. Catal. B Environ.* **2019**, *243*, 36–46. [CrossRef]
34. Muravev, V.; Spezzati, G.; Su, Y.Q.; Parastaev, A.; Chiang, F.K.; Longo, A.; Escudero, C.; Kosinov, N.; Hensen, E.J.M. Interface dynamics of Pd–CeO₂ single-atom catalysts during CO oxidation. *Nat. Catal.* **2021**, *4*, 469–478. [CrossRef]
35. Bazin, P.; Saur, O.; Lavalley, J.C.; Daturi, M.; Blanchard, G. FT-IR study of CO adsorption on Pt/CeO₂: Characterisation and structural rearrangement of small Pt particles. *Phys. Chem. Chem. Phys.* **2005**, *7*, 187–194. [CrossRef]
36. Craciun, R.; Daniell, W.; Knözinger, H. The effect of CeO₂ structure on the activity of supported Pd catalysts used for methane steam reforming. *Appl. Catal. A Gen.* **2002**, *230*, 153–168. [CrossRef]
37. Colinot, F.; Meunier, F.; Daturi, M. Low temperature oxidation catalysis for diesel engine emission control by FT-IR. *Spectrosc. Eur.* **2009**, *21*, 9–12.
38. Bensalem, A.; Muller, J.; Tessier, D.; Bozon-verduraz, F. Spectroscopic study of CO adsorption on palladium-ceria catalysts. *J. Chem. Soc.* **1996**, *92*, 3233–3237.
39. Binet, C.; Jadi, A.; Lavalley, J.C.; Boutonnet-Kizling, M. Metal-support interaction in Pd/CeO₂ catalysts: Fourier-transform infrared studies of the effects of the reduction temperature and metal loading. Part 1.—Catalysts prepared by the microemulsion technique. *J. Chem. Soc. Faraday Trans.* **1992**, *88*, 2079–2084. [CrossRef]
40. Badri, A.; Binet, C.; Lavalley, J.C. Metal-support interaction in Pd/CeO₂ catalysts. Part 2.—Ceria textural effects. *J. Chem. Soc. Faraday Trans.* **1996**, *92*, 1603–1608. [CrossRef]
41. Tereshchenko, A.; Polyakov, V.; Guda, A.; Lastovina, T.; Pimonova, Y.; Bulgakov, A.; Tarasov, A.; Kustov, L.; Butova, V.; Trigub, A.; et al. Ultra-Small Pd Nanoparticles on Ceria as an Advanced Catalyst for CO Oxidation. *Catalysts* **2019**, *9*, 385. [CrossRef]
42. Hu, Z.; Liu, X.; Meng, D.; Guo, Y.; Guo, Y.; Lu, G. Effect of Ceria Crystal Plane on the Physicochemical and Catalytic Properties of Pd/Ceria for CO and Propane Oxidation. *ACS Catal.* **2016**, *6*, 2265–2279. [CrossRef]
43. Wang, G.; Meng, M.; Zha, Y.; Ding, T. High-temperature close coupled catalysts Pd/Ce-Zr-M/Al₂O₃ (M = Y, Ca or Ba) used for the total oxidation of propane. *Fuel* **2010**, *89*, 2244–2251. [CrossRef]
44. Li, M.; Weng, D.; Wu, X.; Wan, J.; Wang, B. Importance of re-oxidation of palladium by interaction with lanthana for propane combustion over Pd/Al₂O₃ catalyst. *Catal. Today* **2013**, *201*, 19–24. [CrossRef]
45. Luo, J.Y.; Meng, M.; Yao, J.S.; Li, X.G.; Zha, Y.Q.; Wang, X.; Zhang, T.Y. One-step synthesis of nanostructured Pd-doped mixed oxides MO_x-CeO₂ (M = Mn, Fe, Co, Ni, Cu) for efficient CO and C₃H₈ total oxidation. *Appl. Catal. B Environ.* **2009**, *87*, 92–103. [CrossRef]